

Electrical detection of the inverse Edelstein effect on the surface of SmB_6

Jehyun Kim¹, Chaun Jang², Xiangfeng Wang³, Johnpierre Paglione³, Seokmin Hong²,

Shehrin Sayed⁴, Dongwon Chun⁵ and Dohun Kim^{1*}

¹Department of Physics and Astronomy, and Institute of Applied Physics, Seoul National University, Seoul 08826, Korea

²Center for Spintronics, Korea Institute of Science and Technology, Seoul 02792, Korea

³Maryland Quantum Materials Center, Department of Physics, University of Maryland, College Park, MD 20742, USA

⁴Electrical Engineering and Computer Science, University of California, Berkeley, California 94720, USA

⁵Advanced Analysis Center, Korea Institute of Science and Technology, Seoul 02792, Korea

*Corresponding author: dohunkim@snu.ac.kr

ABSTRACT: We report the measurement of spin current induced charge accumulation, the inverse Edelstein effect (IEE), on the surface of a candidate topological Kondo insulator SmB_6

single crystal. Robust surface conduction channel of SmB_6 has been shown to exhibit large degree of spin-momentum locking, and spin polarized current through an external ferromagnetic contact induces the spin dependent charge accumulation on the surface of SmB_6 . The dependences of the IEE signal on the bias current, an external magnetic field direction and temperature are consistent with the anticlockwise spin texture for the surface band in SmB_6 in the momentum space, and the direction and magnitude of the effect compared with the normal Edelstein signal are clearly explained by the Onsager reciprocal relation. Furthermore, we estimate spin-to-charge conversion efficiency, the IEE length, as 4.46 nm that is an order of magnitude larger than the efficiency found in other typical Rashba interfaces, implying that the Rashba contribution to the IEE signal could be small. Building upon existing reports on the surface charge and spin conduction nature on this material, our results provide additional evidence that the surface of SmB_6 supports spin polarized conduction channel.

I. INTRODUCTION

Three-dimensional (3D) topological insulators (TIs) are newly developed class of insulators having the bulk band gap in which time-reversal symmetry-protected surface states reside. The surface conduction channel also has spin-momentum locking property making TIs a promising platform for exploring new physics such as Majorana quasi particle states or application to various spintronic devices [1-3]. In the conventional 3D TIs, however, the Fermi level naturally resides in the bulk conduction or valence band due to unintentional doping so that bulk carriers hinders the surface-driven phenomena [4-6]. Recently, SmB_6 , a Kondo insulator, has been predicted to be a member of a newly classified family of strong TIs, topological Kondo insulators (TKIs), where the topologically protected surface states reside in the bulk Kondo band gap at low temperatures,

and the Fermi level is guaranteed to be inside the bulk gap [7-9]. The large degree of current-induced spin polarization on the surface of SmB_6 as well as the robust surface conduction have been demonstrated by various experiments [10-19], implying that the SmB_6 is a strong candidate for TKI free from bulk effects.

Here, we report an additional demonstration that the surface of SmB_6 indeed exhibits transport phenomena consistent with spin-momentum locking texture through the observation of the spin current induced charge accumulation, the inverse Edelstein effect (IEE). Being distinct from the previous experiment for the spin injection into the SmB_6 surface using the microwave-induced spin pumping [11], we use near dc electrical method to generate the charge accumulation by the IEE on the surface of SmB_6 , which can be achieved by not only injection of the spin polarized current generated by the ferromagnetic metal into the surface of SmB_6 , but also extraction of the spin polarized current generated from the surface of SmB_6 . The charge accumulation on the surface of SmB_6 is measured in the form of the voltage difference between two nonmagnetic contacts on the surface, and its dependences on the direction and magnitude of a bias current, external magnetic field direction, and temperature are all consistent with the spin-momentum locking properties of the surface state of SmB_6 .

II. MATERIALS AND METHODS

A. Material growth

Single crystals of SmB_6 were grown with Al flux, starting from elemental Sm and B with the stoichiometry of 1 to 6 in a ratio of $\text{SmB}_6 : \text{Al} = 1 : 200\text{--}250$. The initial materials were placed in an alumina crucible and loaded in a tube furnace under Ar atmosphere. The assembly was heated to $1250\text{--}1400^\circ\text{C}$ and maintained at that temperature for 70–120 hours, then cooled at -2°C/hr to

600–900 °C, followed by faster cooling. The SmB₆ samples were put into sodium hydroxide to remove the residual Al flux.

B. Device fabrication

An Al layer of 2 nm was deposited on the polished (100) surface of SmB₆ by using electron beam evaporation followed by oxidizing on a hotplate in ambient conditions. The resulting thin Al oxide layer prevents direct contact of the ferromagnetic metal with SmB₆ and acts as a tunnel barrier between SmB₆ and the ferromagnetic metal generally enhancing spin injection and detection ratio overcoming conductance mismatch [20] (see Supplementary Information S1). Standard e-beam lithography was used to make electrode patterns. A permalloy (Py) layer was used as a ferromagnetic spin source for spin injection and extraction with the lateral size of 150 x 150 μm^2 and thickness of 20 nm. The layer was capped with 15 nm of Au using electron beam evaporation. Non-ferromagnetic contacts used for the source, drain, and voltage probes were formed by e-beam lithography patterning and Al oxide etching with a buffered oxide etchant followed by depositing Ti 5 nm/Au 80 nm using electron beam evaporation. For the Au electrode acting as the wire bonding pad for the contact with the ferromagnetic metal, additional insulating layer was made below the metal layer by overdosing electron beam on electron beam resist (PMMA 950A6) with a dose of 10000 $\mu\text{C}/\text{cm}^2$.

C. Transport measurements

The device was placed in a commercial variable temperature cryostat (Quantum Design PPMS) for low-temperature electrical measurements. For all electrical measurement, standard lock-in-based four-point probe measurements were performed. An AC current was applied through the

interfacial tunnel oxide between the ferromagnetic metal Py and SmB₆ surface using ac current source (Keithley 6221), and a lock-in amplifier (Stanford Research Systems SR830) was used for detecting a voltage difference between two Au contacts.

III. RESULTS

A. Principle of electrical measurement for the IEE

The Edelstein effect is one of the well-known effects involving charge-to-spin conversion intimately related to the spin Hall effect. In the materials with the spin-momentum locking property, a charge current produces non-equilibrium spin polarization by the Edelstein effect [21]. The Onsager reciprocal effect of the Edelstein effect is called the IEE where a non-equilibrium spin accumulation in a two-dimensional electron gas generates charge accumulation perpendicular to its spin direction [22,23].

To detect a charge accumulation on the surface of SmB₆ arising from the IEE, a permalloy (Py) is used as a spin source to induce a non-equilibrium spin accumulation on the surface of the SmB₆. Figure 1(a) shows the electrical measurement configuration for the IEE, where a bias current I_b flows through Py on the SmB₆ parallel to the y axis, and the transverse voltage difference V_{yx} , defined as $V_+ - V_-$, is measured between two nonmagnetic Au contacts positioned at the end of the SmB₆ in the x axis while sweeping an external magnetic field along the y axis. When measuring V_{yx} , the measured V_{yx} can be classified into four cases according to the direction of I_b and the magnetization of Py (\mathbf{M}).

Figures 1(b)-(e) show schematic top view of the device illustrated in Fig. 1(a) and the charge accumulation by the IEE along the x axis, where the accumulated electrons with spin-up (spin-down) are depicted in red (blue) arrow parallel (anti-parallel) to the +y direction. We note that a

diffusive spin current with the spin anti-parallel to the accumulated spin should flow in the direction opposite to the direction of the charge accumulation due to the zero net current along the x axis. Since the direction of the majority spin of Py is opposite to that of its magnetization and the majority spin of Py is mainly coupled to the SmB₆ surface channel, the contact resistance between Py and spin-up channel of the SmB₆ is larger (smaller) than that between Py and spin-down channel of the SmB₆ for \mathbf{M} parallel to the +y (-y) direction [24,25].

In the case of injection (I_b parallel to the -y direction) in which the spin polarized electrons are injected into the surface of the SmB₆, for \mathbf{M} parallel to the +y (-y) direction, more spin-down (spin-up) electrons are accumulated on the surface of the SmB₆ and subsequently have net momentum in the -x (+x) direction due to the spin-momentum locking, resulting in higher electrochemical potential at left (right) side and, eventually, $V_{yx} < (>) 0$. On the other hand for extraction (I_b parallel to the +y direction) where the spin polarized electrons from the SmB₆ are extracted and tunnel into Py, for \mathbf{M} parallel to the +y (-y) direction, more spin-up (spin-down) electrons are left behind on the surface of the SmB₆ due to high contact resistance, and subsequently have net momentum in the +x (-x) direction due to the spin-momentum locking, resulting in higher electrochemical potential at right (left) side and, eventually, $V_{yx} > (<) 0$. We confirm the non-zero V_{yx} induced by spin current injection/extraction using the simulation based on the semi-classical model for charge and spin transport (see Supplementary Information S2). Summarizing, expected behaviour of V_{yx} as a function of an external magnetic field H_y for injection and extraction is described in the Fig. 1(f) and 1(g), respectively, where H_c is the switching field of Py and the IEE signal ΔV_{yx} , defined as $V_{yx}(\mathbf{M} // +y) - V_{yx}(\mathbf{M} // -y)$, is negative (positive) for injection (extraction). We also define the polarity of the hysteresis loop in Fig. 1(f) and 1(g) as negative and positive polarity, respectively.

B. Electrical measurement of the IEE signal and the Onsager reciprocal relation

We first report the expected behaviour of aforementioned IEE signal on the surface of SmB₆, which is reflected in a non-zero ΔV_{yx} . As shown in Fig. 2(a), V_{yx} is measured by sweeping an external magnetic field along the y axis to control the magnetization direction of Py while applying I_b along the y axis. Figures 2(b) and 2(c) show representative V_{yx} as a function of H_y recorded with I_b of +150 μA and -150 μA , respectively, at 1.8 K. For I_b of +150 μA (-150 μA), the case of extraction (injection), the results show hysteresis loop with positive (negative) polarity according to our expectation, which is clearly consistent with the anticlockwise spin-momentum relation in SmB₆ (see Supplementary Information S3). Being extracted from hysteresis loop under different I_b , as shown in Fig. 2(d), ΔV_{yx} exhibits linear response to I_b , implying that the current-induced spin injection and extraction lead to non-zero ΔV_{yx} .

The IEE signal also can be analysed quantitatively using the Onsager reciprocal relation. The Onsager reciprocal relation is the universal relation for any setup in the linear response regime, stating that the ratio of the measured voltage to a bias current does not change even when exchanging voltage and current terminals [25,26]. However, for time-reversal symmetry breaking field such as \mathbf{M} , the sign of that field should be reversed to satisfy the reciprocity relation. Thus, the Onsager reciprocal relation is given by

$$\frac{V_{12}(\mathbf{M})}{I_{34}} = \frac{V_{34}(-\mathbf{M})}{I_{12}}, \quad (1)$$

where V_{ab} is defined as $V_a - V_b$ and I_{cd} denotes that a current flows from terminal c to terminal d. Figure 3 clearly shows the Onsager reciprocal relation expressed by Eq. (1) between the potentiometric spin measurement, where the ferromagnetic metal is used as the spin detector, and its reciprocal measurement for the IEE, where SmB₆ is used as the spin detector. Figures 3(a) and 3(c) show schematic drawings for the potentiometric spin measurement and the corresponding result, V_{xy} , recorded with I_{12} of 100 μA at 1.8 K while sweeping an external magnetic field along

the y axis. Figures 3(b) and 3(d) also show schematic drawings for the IEE measurement and the corresponding result, V_{yx} , recorded with I_{34} of 100 μA at 1.8 K while sweeping an external magnetic field along the y axis. Each result shows hysteresis loop with negative polarity for the potentiometric measurement and with positive polarity for the IEE measurement consistent with the Onsager reciprocal relation in Eq. (1). More specifically, in the potentiometric spin measurement, the spin voltage ΔV_{xy} can be expressed as follows [27].

$$\frac{\Delta V_{xy}}{I_{12}} = \frac{\Delta V_{34}}{I_{12}} = \frac{V_{34}(\mathbf{M}) - V_{34}(-\mathbf{M})}{I_{12}} = R_B P_{\text{FM}}(\mathbf{p} \cdot \mathbf{M}_{\mathbf{u}}), \quad (2)$$

where ΔV_{xy} is a reciprocal value of ΔV_{yx} in this paper, and proportional to a bias current I_{12} , ballistic resistance of the channel R_B , spin polarization of the ferromagnetic metal P_{FM} , and inner product between the spin polarization of the surface channel with a positive bias current flowing \mathbf{p} and unit vector along the magnetization of the ferromagnetic metal $\mathbf{M}_{\mathbf{u}}$. Eq. (1) and Eq. (2) can be combined to yield the following equation.

$$\frac{\Delta V_{yx}}{I_{34}} = \frac{\Delta V_{12}}{I_{34}} = \frac{V_{12}(\mathbf{M}) - V_{12}(-\mathbf{M})}{I_{34}} = -R_B P_{\text{FM}}(\mathbf{p} \cdot \mathbf{M}_{\mathbf{u}}), \quad (3)$$

where the negative sign arises in order to satisfy the Onsager reciprocal relation. As expected in Eq. (3), the slope from linear fitting shown in Fig. 2(d) has opposite sign compared to that of the bias current dependence of the spin voltage [19,28]. Furthermore, the magnitude of the slope in Fig. 2(d) is 2.7 m Ω slightly larger than the previous value 2.3 m Ω measured in the potentiometric geometry previously performed [19], which may be attributed to the non-linearity of the contact resistance between the ferromagnetic metal and SmB₆. As the IEE signal follows the Onsager reciprocal relation, we estimate both from inverse and normal Edelstein effect that $|\mathbf{p}|$ of SmB₆ is 27% (see Supplementary Information S4). Therefore, the IEE signal ΔV_{yx} electrically measured

through both spin injection and extraction supports that SmB₆ indeed has the anticlockwise surface spin texture in the momentum space.

C. Magnetization orientation dependence of the IEE signal

To further confirm the spin-momentum relation, we study how the IEE signal depends on the magnetization orientation. Figures 4(a) and 4(b) show schematic top view of measurement configuration when applying an external magnetic field along the y axis and x axis, respectively, under I_b of 100 μ A at 1.8 K and corresponding results are shown in Fig. 4(c) and 4(d). Due to the anticlockwise spin texture for the surface band in SmB₆, the charge accumulation by spin-to-charge conversion on the surface of SmB₆ occurs along the x axis as depicted in Fig. 4(a), resulting in measurable ΔV_{yx} as shown in Fig. 4(c). On the other hand, we can predict that the charge accumulation occurs along the y axis in case of \mathbf{M} parallel to x axis as depicted in Fig. 4(b), resulting in no voltage difference between two voltage probes at high positive or negative H_x as shown in Fig. 4(d). The intermittent non-zero signal in Fig. 4(d) likely arises from the magnetic domain, whose transient magnetization direction has some y axis component in the process of magnetization reversal through the domain wall motion [29]. Furthermore, the result in Fig. 4(d) also exclude the possibility that the measured ΔV_{yx} could originate from spurious effects such as Hall effect where non-zero ΔV_{yx} can arise independently of the magnetization orientation due to the fringe field of the ferromagnetic injector [30]. Therefore, magnetization dependences of the IEE signal further support the fact that the measured ΔV_{yx} clearly reflects the anticlockwise spin texture for the surface band in SmB₆.

D. Temperature dependence of the IEE signal

The surface origin of ΔV_{yx} is examined by investigating the temperature dependence of ΔV_{yx} . As shown in Fig. 5(a), the temperature-dependent electrical resistance $R(T)$ of SmB₆ diverges from

12 K to 4 K exhibiting thermally activated behaviour and starts to saturate at 4 K exhibiting the surface-dominated transport property, as previously confirmed [16-18]. Fig. 5(b) shows V_{yx} as a function of H_y under I_b of +100 μA performed at temperature ranging from 4.5 K to 1.8 K [marked by red dots in Fig. 5(a)]. The IEE signal ΔV_{yx} is extracted from Fig. 5(b) and summarized in Fig. 5(c) according to the temperature where the measurement is performed. As the temperature increases, ΔV_{yx} constantly decreases and vanishes around 4 K, which resemble the behaviour of the temperature-dependent electrical resistance of SmB_6 showing the crossover from surface to bulk-dominated charge conduction around 4 K. Moreover, although SmB_6 is a heavy metal where spin Hall and inverse spin Hall effect can occur, the signal from inverse spin Hall effect does not contribute to the measured ΔV_{yx} at the elevated temperature, which may be largely attributed to thick bulk channel of SmB_6 because the inverse spin Hall signal diminishes with the thickness of the spin detector material increasing due to the reduction of the spatially averaged spin current in the spin detector material [31]. We also note that the temperature dependences of the measured ΔV_{yx} exhibit the similar behaviour to the previous results of the temperature-dependent ΔV_{xy} in the potentiometric measurement configuration, confirming the Onsager reciprocal relation is valid with varying temperature [19]. Therefore, the temperature dependences of the measured ΔV_{yx} strongly support that the measured ΔV_{yx} indeed originates from the surface states of SmB_6 largely excluding the bulk effect such as the inverse spin Hall effect.

IV. DISCUSSION

The location of the Fermi energy pinned near the hybridization-induced gap induced by hybridization of localized f electrons with conduction electrons ensures surface-dominated transport in SmB_6 at low temperatures [17,18], thereby excluding the possibility that the bulk

effects such as inverse spin Hall effect contribute to the measured IEE signal. However, the IEE signal can arise from both the Rashba surface states and the topologically protected surface states because both surface states have the spin-momentum locking property which can induce the IEE signal. Although it is hard to separately measure the contributions of the Rashba surface and the topological surface to the IEE signal, we can predict that the measured IEE signal is very likely to consist mainly of the signal from the topological surface by analyzing the IEE length, λ_{IEE} , which is spin-to-charge conversion efficiency given by the following equation [24,32].

$$j_C = \lambda_{\text{IEE}} j_S, \quad \lambda_{\text{IEE}} = \frac{|\mathbf{p}| \lambda}{\pi}, \quad (4)$$

where charge current density in A m^{-1} , j_C , and spin current density in A m^{-2} , j_S , are connected through λ_{IEE} that is proportional to absolute value of the spin polarization $|\mathbf{p}|$ and mean free path of the channel λ . In SmB_6 , because β band electrons mainly contribute to surface conduction, λ for β band (52 nm) [33] and the spin polarization (27%) are used to obtain λ_{IEE} . In our case, λ_{IEE} is 4.46 nm, which is comparable to λ_{IEE} found in α -Sn films topological insulator without bulk effects [34] and one order larger than λ_{IEE} found in various other Rashba interfaces, typically 0.1-0.4 nm due to the compensation of the two Fermi contours of Rashba interfaces [35-39], implying that the Rashba contribution to the IEE signal could be small. Moreover, large λ_{IEE} also indicates that SmB_6 is promising candidate for spintronic devices potentially useful for efficient spin source and detector. With recently developed technique of increasing temperature range of surface-dominated transport in SmB_6 by applying strain [40], the material also has potential for spintronic application at elevated temperature. Our observation can present a route for the potential application of SmB_6 to both fundamental investigation of the interplay between nontrivial topology and electron correlation and applied spin transport physics in strongly correlated system.

ACKNOWLEDGMENT

This research was supported by the Basic Science Research Program (Grant No. NRF-2015R1C1A1A02037430 and 2018R1A2A3075438) through the National Research Foundation of Korea (NRF) funded by the Ministry of Science, ICT and Future Planning, and Creative-Pioneering Researchers Program through Seoul National University(SNU). Research at the University of Maryland was supported by the Gordon and Betty Moore Foundation's EPIQS Initiative through Grant No. GBMF9071, and the Maryland Quantum Materials Center. Electrical measurements used shared facilities funded by the KIST institutional program and the National Research Council of Science&Technology (NST) grant (No. CAP-16-01-KIST). J.K. and C.J. contributed equally to this work.

REFERENCES

- [1] A. R. Akhmerov, J. Nilsson, and C. W. J. Beenakker, *Electrically Detected Interferometry of Majorana Fermions in a Topological Insulator*, Phys. Rev. Lett. **102**, 216404 (2009).
- [2] L. Fu and C. L. Kane, *Superconducting proximity effect and Majorana fermions at the surface of a topological insulator*, Phys. Rev. Lett. **100**, 096407 (2008).
- [3] J. H. Han, A. Richardella, S. A. Siddiqui, J. Finley, N. Samarth, and L. Q. Liu, *Room-Temperature Spin-Orbit Torque Switching Induced by a Topological Insulator*, Phys. Rev. Lett. **119**, 077702 (2017).
- [4] D. Hsieh *et al.*, *A tunable topological insulator in the spin helical Dirac transport regime*, Nature **460**, 1101 (2009).
- [5] D. S. Kong *et al.*, *Rapid Surface Oxidation as a Source of Surface Degradation Factor for Bi₂Se₃*, ACS Nano **5**, 4698 (2011).
- [6] D. Kim, S. Cho, N. P. Butch, P. Syers, K. Kirshenbaum, S. Adam, J. Paglione, and M. S. Fuhrer, *Surface conduction of topological Dirac electrons in bulk insulating Bi₂Se₃*, Nat. Phys. **8**, 459 (2012).
- [7] R. Yu, H. M. Weng, Z. Fang, and X. Dai, *Pseudospin, real spin, and spin polarization of photoemitted electrons*, Phys. Rev. B **94**, 085123 (2016).
- [8] R. Yu, H. M. Weng, X. Hu, Z. Fang, and X. Dai, *Model Hamiltonian for topological Kondo insulator SmB₆*, New J. Phys. **17**, 023012 (2015).

- [9] M. Dzero, K. Sun, V. Galitski, and P. Coleman, *Topological Kondo Insulators*, Phys. Rev. Lett. **104**, 106408 (2010).
- [10] J. Jiang *et al.*, *Observation of possible topological in-gap surface states in the Kondo insulator SmB_6 by photoemission*, Nat. Commun. **4**, 3010 (2013).
- [11] Q. Song *et al.*, *Spin injection and inverse Edelstein effect in the surface states of topological Kondo insulator SmB_6* , Nat. Commun. **7**, 13485 (2016).
- [12] N. Xu *et al.*, *Direct observation of the spin texture in SmB_6 as evidence of the topological Kondo insulator*, Nat. Commun. **5**, 4566 (2014).
- [13] D. J. Kim, J. Xia, and Z. Fisk, *Topological surface state in the Kondo insulator samarium hexaboride*, Nat. Mater. **13**, 466 (2014).
- [14] Y. Nakajima, P. Syers, X. F. Wang, R. X. Wang, and J. Paglione, *One-dimensional edge state transport in a topological Kondo insulator*, Nat. Phys. **12**, 213 (2016).
- [15] M. Neupane *et al.*, *Surface electronic structure of the topological Kondo-insulator candidate correlated electron system SmB_6* , Nat. Commun. **4**, 2991 (2013).
- [16] S. Wolgast, C. Kurdak, K. Sun, J. W. Allen, D. J. Kim, and Z. Fisk, *Low-temperature surface conduction in the Kondo insulator SmB_6* , Phys. Rev. B **88**, 180405 (2013).
- [17] D. J. Kim, S. Thomas, T. Grant, J. Botimer, Z. Fisk, and J. Xia, *Surface Hall Effect and Nonlocal Transport in SmB_6 : Evidence for Surface Conduction*, Sci. Rep. **3**, 3150 (2013).
- [18] P. Syers, D. Kim, M. S. Fuhrer, and J. Paglione, *Tuning Bulk and Surface Conduction in the Proposed Topological Kondo Insulator SmB_6* , Phys. Rev. Lett. **114**, 096601 (2015).
- [19] J. Kim, C. Jang, X. F. Wang, J. Paglione, S. Hong, J. Lee, H. Choi, and D. Kim, *Electrical detection of the surface spin polarization of the candidate topological Kondo insulator SmB_6* , Phys. Rev. B **99**, 245148 (2019).
- [20] E. I. Rashba, *Theory of electrical spin injection: Tunnel contacts as a solution of the conductivity mismatch problem*, Phys. Rev. B **62**, R16267 (2000).
- [21] V. M. Edelstein, *SPIN POLARIZATION OF CONDUCTION ELECTRONS INDUCED BY ELECTRIC-CURRENT IN 2-DIMENSIONAL ASYMMETRIC ELECTRON-SYSTEMS*, Solid State Communications **73**, 233 (1990).
- [22] K. Shen, G. Vignale, and R. Raimondi, *Microscopic Theory of the Inverse Edelstein Effect*, Phys. Rev. Lett. **112**, 096601 (2014).
- [23] R. Dey, L. F. Register, and S. K. Banerjee, *Modeling all-electrical detection of the inverse Edelstein effect by spin-polarized tunneling in a topological-insulator/ferromagnetic-metal heterostructure*, Phys. Rev. B **97**, 144417 (2018).
- [24] S. Sayed, S. Hong, and S. Datta, *Multi-Terminal Spin Valve on Channels with Spin-Momentum Locking*, Sci. Rep. **6**, 35658 (2016).
- [25] J. H. Lee, H. J. Kim, J. Chang, S. H. Han, H. C. Koo, S. Sayed, S. Hong, and S. Datta, *Multi-terminal spin valve in a strong Rashba channel exhibiting three resistance states*, Sci. Rep. **8**, 3397 (2018).
- [26] P. Jacquod, R. S. Whitney, J. Meair, and M. Buttiker, *Onsager relations in coupled electric, thermoelectric, and spin transport: The tenfold way*, Phys. Rev. B **86**, 155118 (2012).
- [27] S. Hong, V. Diep, S. Datta, and Y. P. Chen, *Modeling potentiometric measurements in topological insulators including parallel channels*, Phys. Rev. B **86**, 085131 (2012).
- [28] L. Q. Liu, A. Richardella, I. Garate, Y. Zhu, N. Samarth, and C. T. Chen, *Spin-polarized tunneling study of spin-momentum locking in topological insulators*, Phys. Rev. B **91**, 235437 (2015).

- [29] D. Romel, E. R. Burke, and I. D. Mayergoyz, *Magnetic imaging in the presence of external fields: Technique and applications*, Journal of Applied Physics **79**, 6441 (1996).
- [30] E. K. de Vries, A. M. Kamerbeek, N. Koirala, M. Brahlek, M. Salehi, S. Oh, B. J. van Wees, and T. Banerjee, *Towards the understanding of the origin of charge-current-induced spin voltage signals in the topological insulator Bi_2Se_3* , Phys. Rev. B **92**, 201102(R) (2015).
- [31] V. Castel, N. Vlietstra, J. Ben Youssef, and B. J. van Wees, *Platinum thickness dependence of the inverse spin-Hall voltage from spin pumping in a hybrid yttrium iron garnet/platinum system*, Applied Physics Letters **101**, 132414 (2012).
- [32] S. Sayed, S. Hong, and S. Datta, *Transmission-Line Model for Materials with Spin-Momentum Locking*, Physical Review Applied **10**, 054044 (2018).
- [33] G. Li *et al.*, *Two-dimensional Fermi surfaces in Kondo insulator SmB_6* , Science **346**, 1208 (2014).
- [34] J. C. Rojas-Sanchez *et al.*, *Spin to Charge Conversion at Room Temperature by Spin Pumping into a New Type of Topological Insulator: $\alpha\text{-Sn}$ Films*, Phys. Rev. Lett. **116**, 096602 (2016).
- [35] M. Matsushima, Y. Ando, S. Dushenko, R. Ohshima, R. Kumamoto, T. Shinjo, and M. Shiraishi, *Quantitative investigation of the inverse Rashba-Edelstein effect in Bi/Ag and Ag/Bi on YIG* , Applied Physics Letters **110**, 072404 (2017).
- [36] W. Zhang, M. B. Jungfleisch, W. J. Jiang, J. E. Pearson, and A. Hoffmann, *Spin pumping and inverse Rashba-Edelstein effect in $\text{NiFe}/\text{Ag}/\text{Bi}$ and $\text{NiFe}/\text{Ag}/\text{Sb}$* , Journal of Applied Physics **117**, 17C727 (2015).
- [37] S. Sangiao, J. M. De Teresa, L. Morellon, I. Lucas, M. C. Martinez-Velarte, and M. Viret, *Control of the spin to charge conversion using the inverse Rashba-Edelstein effect*, Applied Physics Letters **106**, 172403 (2015).
- [38] A. Nomura, T. Tashiro, H. Nakayama, and K. Ando, *Temperature dependence of inverse Rashba-Edelstein effect at metallic interface*, Applied Physics Letters **106**, 212403 (2015).
- [39] J. C. Rojas Sanchez, L. Vila, G. Desfonds, S. Gambarelli, J. P. Attane, J. M. De Teresa, C. Magen, and A. Fert, *Spin-to-charge conversion using Rashba coupling at the interface between non-magnetic materials*, Nat. Commun. **4**, 2944 (2013).
- [40] A. Stern, M. Dzero, V. M. Galitski, Z. Fisk, and J. Xia, *Surface-dominated conduction up to 240 K in the Kondo insulator SmB_6 under strain*, Nat. Mater. **16**, 708 (2017).

Figure captions

FIG. 1. Principle of electrical measurement of the Inverse Edelstein Effect (IEE). (a) Schematic of measurement setup and anticlockwise spin texture of the surface band in SmB_6 near the Fermi energy. (b)-(e) Schematic top view for the charge accumulation by the IEE in case of $\mathbf{M} // +y$ under injection (b), $\mathbf{M} // +y$ under extraction (c), $\mathbf{M} // -y$ under injection (d), and $\mathbf{M} // -y$ under extraction (e). (f), (g) The expected inverse Edelstein signal for spin injection (f) and extraction (g).

FIG. 2. Electrical measurement of the IEE signal. (a) Schematic drawing of the electrical measurement configuration. A bias current I_b is applied along the y axis and voltage difference is measured between two Au contacts while sweeping a magnetic field along the y axis. (b), (c) The measured V_{yx} as a function of the y component of an external magnetic field H_y for I_b of +150 μA (b) and -150 μA (c). (d) Dependence of the IEE signal ΔV_{yx} as a function of I_b measured at 1.8 K.

FIG. 3. The Onsager reciprocal relation. (a), (b) Schematic measurement setup for the potentiometric spin measurement (a) and its reciprocal measurement for the IEE (b). (c) V_{xy} , defined as $V_3 - V_4$, as a function of the external magnetic field swept along the y axis under I_{12} of 100 μA at 1.8 K, measured in Fig. 3(a) configuration [19]. (d) V_{yx} , defined as $V_1 - V_2$, as a function of an external magnetic field swept along the y axis under I_{34} of 100 μA at 1.8 K, measured in Fig. 3(b) configuration.

FIG. 4. Magnetization orientation dependence of the IEE signal. (a), (b) Schematic top view of the measurement configuration. An external magnetic field is swept along the y axis in (a) and along the x axis in (b). (c), (d) V_{yx} as a function of an external magnetic field swept along the y

axis (c) and along the x axis (d) under I_b of +100 μA at 1.8 K. Magnetization \mathbf{M} is parallel to the y axis (parallel to current direction) in (c) and parallel to the x axis (perpendicular to current direction) in (d).

FIG. 5. Temperature dependence of the IEE signal. (a) Electrical resistance of SmB_6 as a function of temperature under a bias current of 300 μA . (b) V_{yx} measured by sweeping an external magnetic field parallel to the y axis under a bias current of +100 μA at different temperatures ranging from 1.8 K to 4.5 K. Each curve is offset by 1 μV for clarity. (c) The IEE signal ΔV_{yx} extracted from Fig. 4(b) as a function of temperature.

Figure 1

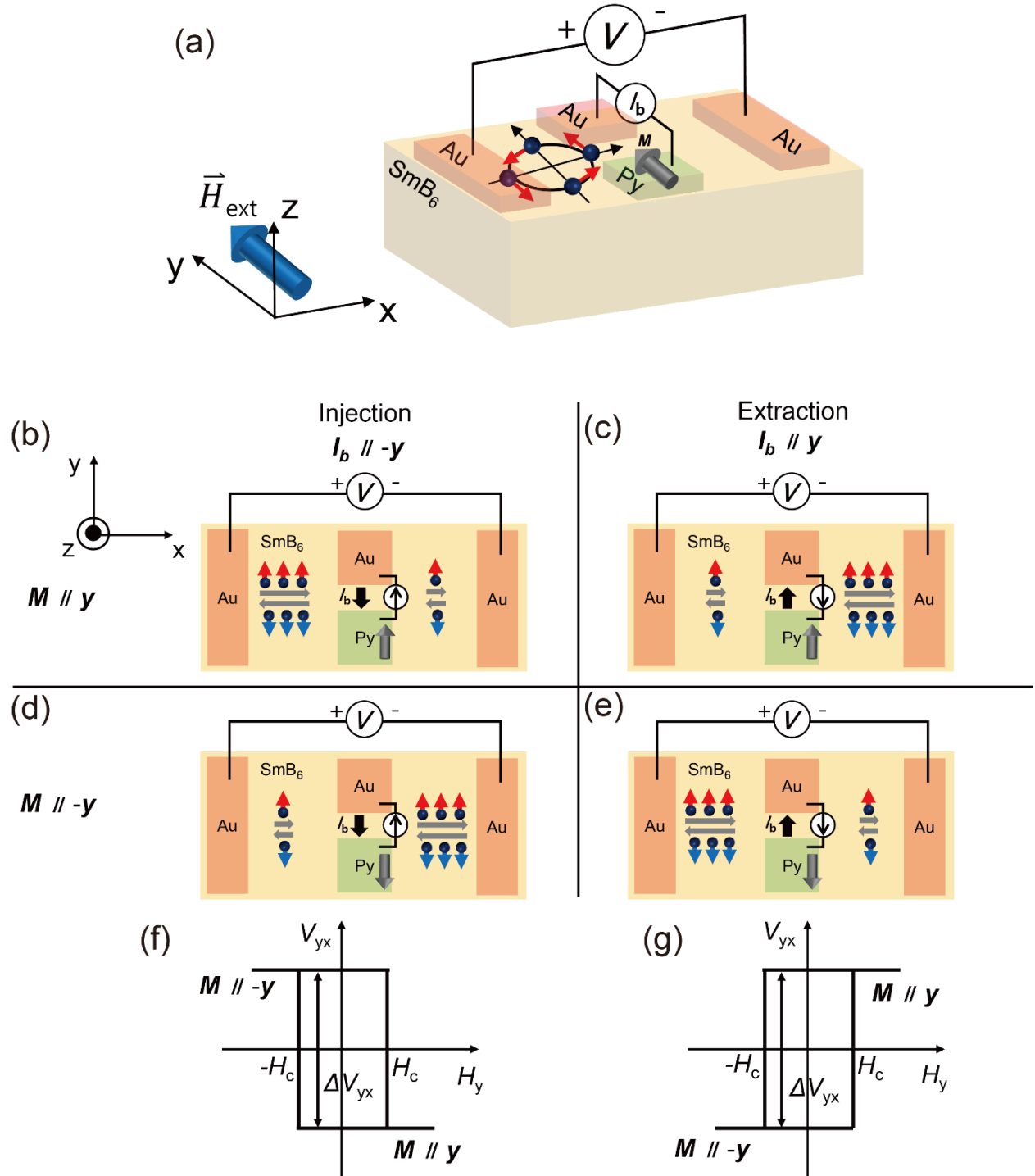


Figure 2

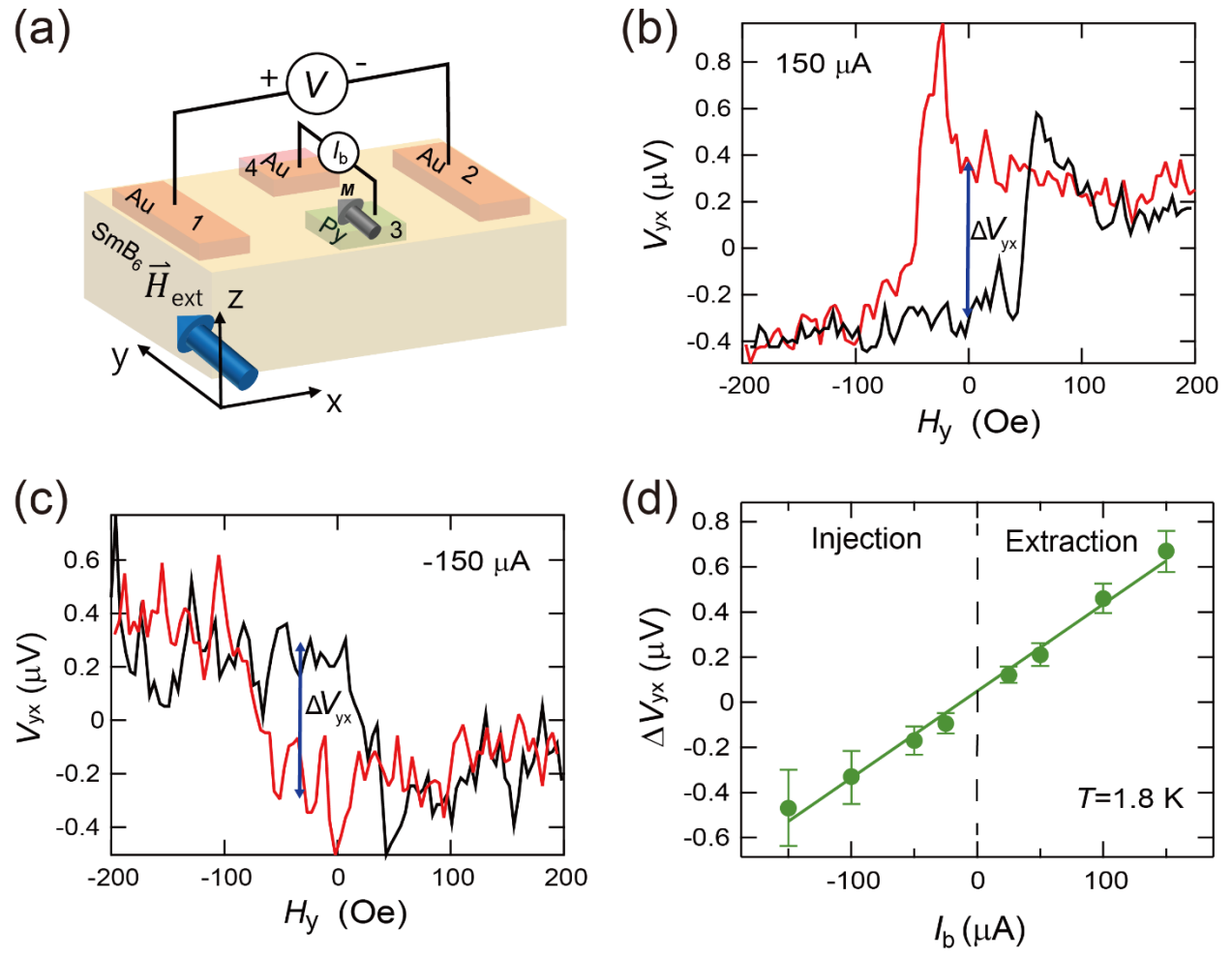


Figure 3

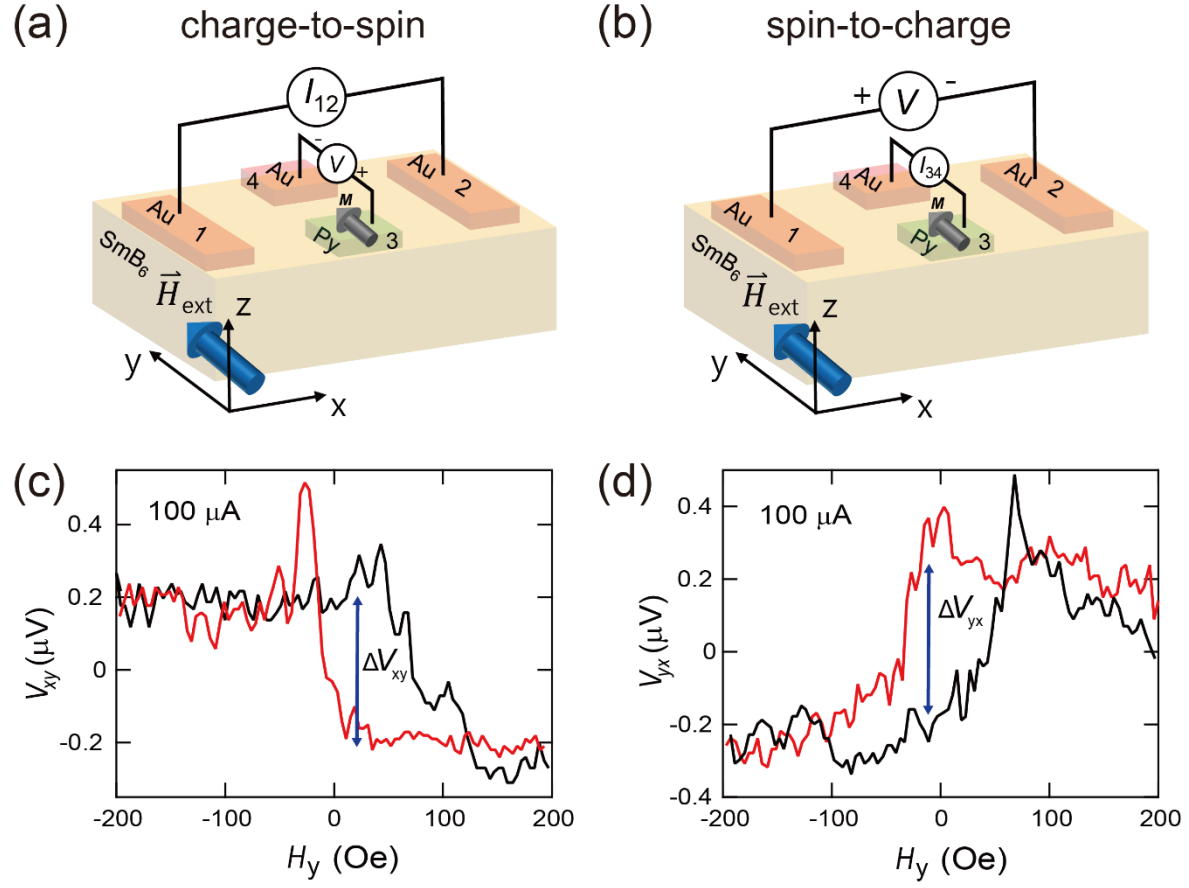


Figure 4

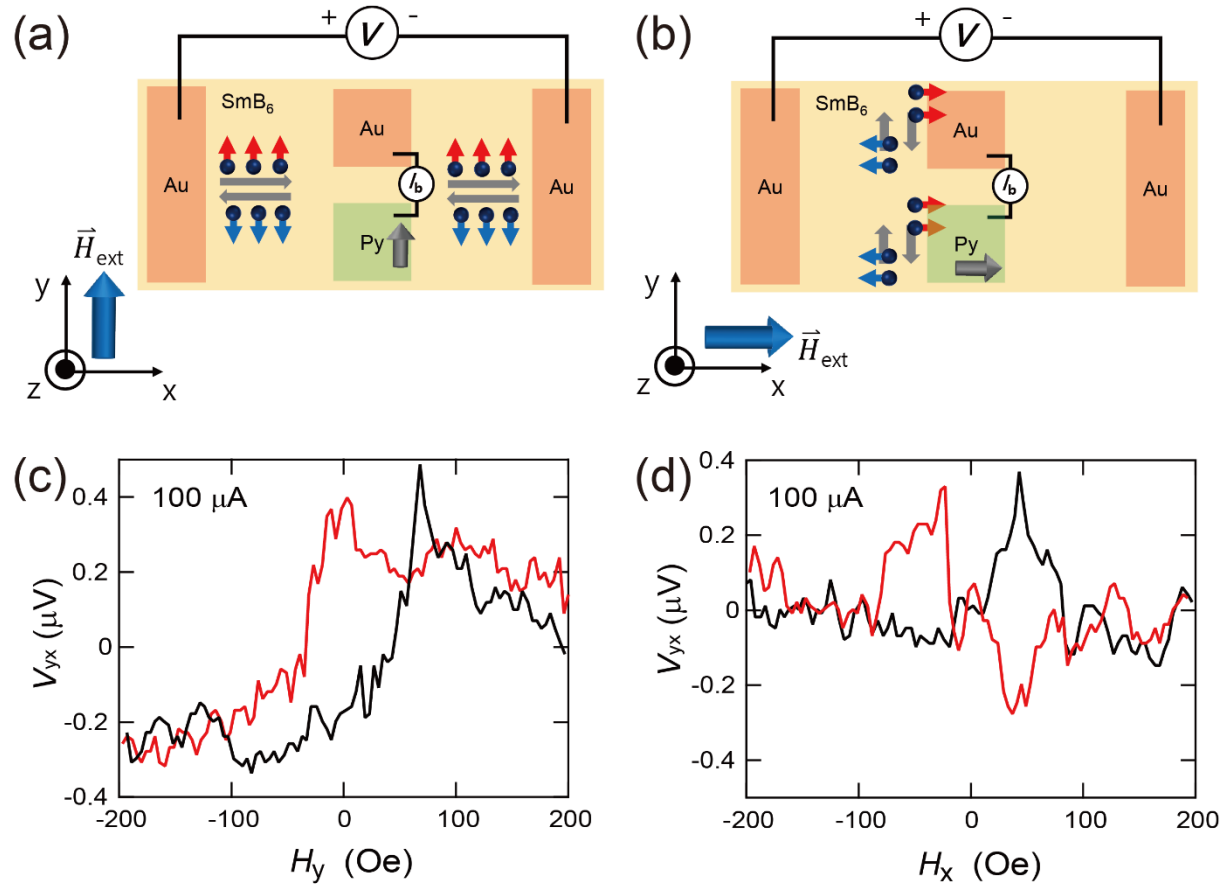


Figure 5

